

Microstructural evolution in semi-solid AA7034

Hee-Soo Kim · Ian C. Stone · Brian Cantor

Received: 5 March 2007 / Accepted: 10 September 2007 / Published online: 4 December 2007
© Springer Science+Business Media, LLC 2007

Abstract The kinetics of semi-solid grain coarsening in a spray-formed AA7034 aluminium alloy were determined by the use of ex situ coarsening experiments. The coarsening rate constant of the alloy decreases with increasing solid fraction for solid fractions greater than 0.65. For solid fractions between 0.6 and 0.65, the coarsening rate constant increases as the solid fraction increases. For solid fractions below 0.6, the coarsening rate constant decreases again with increasing solid fraction. A model of flow-enhanced diffusion was developed to explain the grain-coarsening behaviour at low solid fractions, with flow caused by the macroscopic shape change of the uncontained semi-solid material during coarsening. Together with previous liquid film and modified liquid film migration models, the flow-enhanced diffusion model shows qualitative agreement with available experimental results.

Introduction

Semi-solid forming is a state-of-the-art process for near-net shaping of complex products, which combines elements of casting and forging and has benefits such as enhanced die

life and energy efficiency [1, 2]. The semi-solid forming process requires careful control of the size and morphology of the solid grains, since deformation depends sharply upon initial microstructure, as shown by Han [3]. The size of the solid grains should be minimised and their shape should be spheroidal for better forming ability, e.g., [3]. It is, therefore, important to understand the kinetics and mechanisms controlling the coarsening behaviour of such microstructures.

Semi-solid grain coarsening is also crucial in the spray-forming process, in which a liquid alloy metal stream is atomised into an array of fine droplets by jets of high-pressure inert gas, and then deposits onto the surface of a growing preform to build up large billets, tubes, or rings for down stream processing [4]. The microstructure of the spray-formed preform consists of fine equiaxed grains without microsegregation. The dendrites contained within the droplets break up on impact with the top surface, and then spheroidise and coarsen in a sump of semi-solid material at the top of the growing preform before final solidification [5, 6]. In order to understand the evolution of the spray-formed microstructure, it is important to understand the kinetics of grain coarsening in the semi-solid state. Spray-formed alloys are considered as candidate feedstock materials for semi-solid processing due to their fine equiaxed microstructures [2].

Although there have been a number of analytical and experimental studies of grain coarsening in the semi-solid state [7–11], the mechanisms of grain growth have not yet been described clearly throughout the full range of solid fraction. The most recent general description of grain coarsening in the semi-solid state was given by Manson-Whitton et al. [11]. They suggested that for solid fractions, f_s , less than a critical value of about 0.7, the dominant coarsening mechanism is liquid film migration activated by

H.-S. Kim · I. C. Stone (✉)
Department of Materials, University of Oxford, Parks Road,
Oxford OX1 3PH, UK
e-mail: ian.stone@materials.ox.ac.uk

Present Address:
H.-S. Kim
CAE_G, Central R&D Institute, Samsung Electro-Mechanics,
314 Maetan 3-Dong, Yeongtong-Gu, Suwon, Gyunggi-Do
443-743, Korea

B. Cantor
University of York, Heslington, York YO10 5DD, UK

diffusion across the liquid films between the solid grains. Below the critical value, as the solid fraction increases the diffusion distance between the grains decreases, causing the coarsening rate to increase [8, 11]. On the other hand, for solid fractions greater than the critical value of about 0.7, the dominant coarsening mechanism is referred to as modified liquid film migration, with diffusion across the liquid films deactivated by direct contacts between the solid grains. As the solid fraction increases beyond the critical value, solid grain contacts increase and the area of liquid film reduces, causing the coarsening rate to decrease [11].

The main objective of the present study was to develop a fundamental understanding of the microstructural evolution of materials in the semi-solid state. Conventional *ex situ* grain-coarsening experiments were carried out to validate the kinetics of grain coarsening in the semi-solid state, using spray-formed AA7034 alloy.

Experimental

The material used to study the kinetics of semi-solid grain coarsening and the deformation behaviour in the semi-solid state was a commercial spray-formed aluminium alloy AA7034, the nominal composition of which is 11.0–12.0 Zn, 2.0–3.0 Mg, 0.80–1.20 Cu, 0.08–0.30 Zr, 0.12 max Fe, 0.10 max Si (in wt.%). The actual composition, measured by the supplier, Osprey Metals Ltd, Neath, UK, of the alloy used in this study was Al-9.95Zn-2.23Mg-1.20Cu-0.18Cr-0.18Zr-0.004Mn-0.005Ti-0.04Si-0.16Fe (in wt.%). The AA7034 alloy was chosen because it is the highest strength commercially available alloy, its spray-formed microstructure is fine and highly equiaxed, and therefore of interest for semi-solid processing, and there is very little data on semi-solid grain coarsening of Al-Zn-based systems. The AA7034 alloy was spray formed by Osprey Metals Ltd, Neath, UK, and was in the form of a 30 kg cylindrical preform, approximately 300 mm in diameter and approximately 140 mm in height.

Specimens approximately 10 mm × 10 mm × 10 mm in size were heat treated in the hot zone of a preheated tube furnace at temperatures (within the error of ±1 °C) corresponding to solid fractions of $0.5 \leq f_s \leq 0.9$. Heat treatment times were 15, 30, 60, 120, and 240 min. The relationship between solid fraction and temperature was determined by integration of the melting and solidification peaks from differential scanning calorimetry (DSC) experiments at 20 °C min⁻¹. The heat treatment temperatures and corresponding solid fractions are given in Table 1.

The furnace was preheated to the heat treatment temperatures, which were measured using a K-type

Table 1 Solid fraction–temperature relationship for the spray-formed AA7034 alloy

Solid fraction	Heat treatment temperature (°C)	Solid fraction	Heat treatment temperature (°C)
0.00 (Liquidus)	640	0.55	611
0.05	634	0.60	607
0.10	632	0.65	601
0.15	631	0.70	595
0.20	629	0.75	586
0.25	627	0.80	573
0.30	625	0.85	555
0.35	623	0.90	529
0.40	621	0.95	493
0.45	618	1.00 (Solidus)	463
0.50	615		

thermocouple placed in the centre of the furnace, and allowed to stabilise for at least 2 h prior to heat treatment. Since the distribution of temperature in the furnace was not uniform, the hot zone of the target temperature was determined prior to heat treatment. During the heat treatment, the thermocouple was placed next to the samples. The temperature of the furnace was controlled using this temperature rather than the preset temperature of the furnace. The specimens were quenched in cold water after the heat treatment to “freeze in” the microstructure held in the semi-solid state, although it should be noted that any attempt to estimate solid fraction from the quenched microstructure would over-estimate the actual solid fraction at temperature due to solidification on pre-existing solid grains during the quench. It was difficult to perform the heat treatment at temperatures corresponding to solid fractions lower than 0.5 since solid fraction is very sensitive to temperature in this region.

To observe the microstructure of the initial and heat-treated specimens, the samples were mounted, ground, and polished to a 1 μm finish. The samples were etched in 0.5% HF solution or Keller’s reagent (2.5% HNO₃-1.5% HCl-0.5% HF in H₂O) to reveal the grain boundaries, grain boundary liquid films, and secondary phases. The specimens were observed using a Zeiss Axiophot 2 optical microscope. The grain sizes were measured from the optical micrographs of the initial specimens and the series of optical micrographs of the heat-treated specimens using the mean linear intercept method in which a line of known length was superimposed over the image and the number of grain boundaries cutting that line was counted. The mean grain size of the line is given by the ratio of the number of the grain boundaries to the length of the line. For each sample, measurements were taken from the whole sectioned area except the edge area of the micrograph. About

300–500 grain boundary intercepts were counted per sample. An overall mean value was taken for each sample.

Results

Initial microstructure

Figure 1 is an optical micrograph of as-received spray-formed AA7034. The microstructure consisted of uniformly equiaxed α -Al grains with an average grain size of approximately 43 μm . Fine-scale second-phase particles, $\sim 1 \mu\text{m}$ in size, identified as MgZn_2 by X-ray diffraction, were distributed throughout the grains and at the grain boundaries [12]. There were also some coarse, blocky particles at the grain boundaries and triple points, $\sim 20 \mu\text{m}$ in size, identified as Al_7Cr by electron probe microanalysis [12], as indicated by arrows in Fig. 1.

Microstructures after grain coarsening in the semi-solid state

Figure 2 shows a series of optical micrographs of the AA7034 alloy quenched after heat treatment at a solid fraction of 0.75 for heat treatment times of (a) 30, (b) 60, (c) 120, and (d) 240 min. Figure 3 shows a series of micrographs of the AA7034 alloy quenched after heat treatment for the heat treatment time of 120 min at solid fractions of (a) 0.90 (529 $^\circ\text{C}$), (b) 0.80 (573 $^\circ\text{C}$), (c) 0.70 (595 $^\circ\text{C}$), and (d) 0.60 (607 $^\circ\text{C}$). The microstructures were generally characterised by smooth and rounded grains (labelled SG in Fig. 2d) representing the solid phase in the

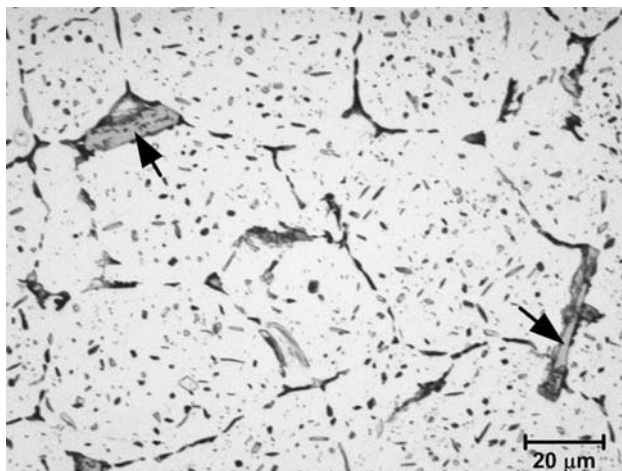


Fig. 1 Optical micrograph of the typical microstructure of the as-received spray-formed AA7034 alloy. The arrows indicate large secondary precipitates at grain boundaries and triple points

semi-solid state. The regions between these solid grains represent the regions of intergranular liquid (or grain boundary liquid film, labelled IL in Fig. 2d) in the semi-solid state. The grain size increased apparently with increasing time. The dark spots inside the grains indicate the positions of intragranular liquid droplets (labelled LD in Fig. 2d), as previously reported for alloy N707 which has a similar composition (Al-10Zn-2Mg-1Cu-0.2Zr in wt.%) to AA7034 [7]. The number of intragranular liquid droplets decreased as the grains coarsened with time. Whilst the intergranular liquid readily wetted most grain boundaries, there existed some unwetted or partially wetted interfaces between solid grains (labelled UW in Fig. 2d) even at the low solid fraction of 0.5. The grains kept their globular shape during the heat treatment.

Figure 4 is a plot of the mean linear intercept grain size against heat treatment time for specimens heat treated at 529–615 $^\circ\text{C}$ ($f_s = 0.90$ –0.50). The figure shows that average grain size increased with increasing heat treatment time at all temperatures. At 529 $^\circ\text{C}$ ($f_s = 0.90$), the grain size coarsened only slightly during 240 min of heat treatment. Otherwise, the mean grain size increased rapidly from the initial grain size, but with a progressively slower rate of coarsening as time increased. That is, the rate of increase of grain size decreased with increasing time.

Discussion

Measured kinetics of grain coarsening in the semi-solid state

The equation for the kinetics of grain growth in the semi-solid state has previously been shown to approximate Ostwald ripening type kinetics of a dispersed second phase [11]:

$$\bar{d}^n - \bar{d}_0^n = Kt \quad (1)$$

where \bar{d} is the average grain size after heat treatment time t , \bar{d}_0 is average initial grain size, K is the temperature-dependent grain-coarsening rate constant, and n is the coarsening exponent.

The driving force for grain growth in the solid state is the reduction of grain boundary area. In this case, grain boundary migration is interface controlled, and Eq. 1 follows parabolic grain growth kinetics ($n = 2$). The driving force for coarsening of solid particles in a solid matrix is the reduction of the particle/matrix interfacial surface area. In this case, interface migration is diffusion controlled, and Eq. 1 follows cubic Ostwald ripening kinetics ($n = 3$).

The kinetics of grain coarsening in the semi-solid state have been shown to approximate the Ostwald ripening kinetics of a dispersed second phase. Although it is often

Fig. 2 Optical micrographs of the spray-formed AA7034 alloy quenched after isothermal heat treatment at 586 °C ($f_S = 0.75$) for (a) 30, (b) 60, (c) 120, and (d) 240 min

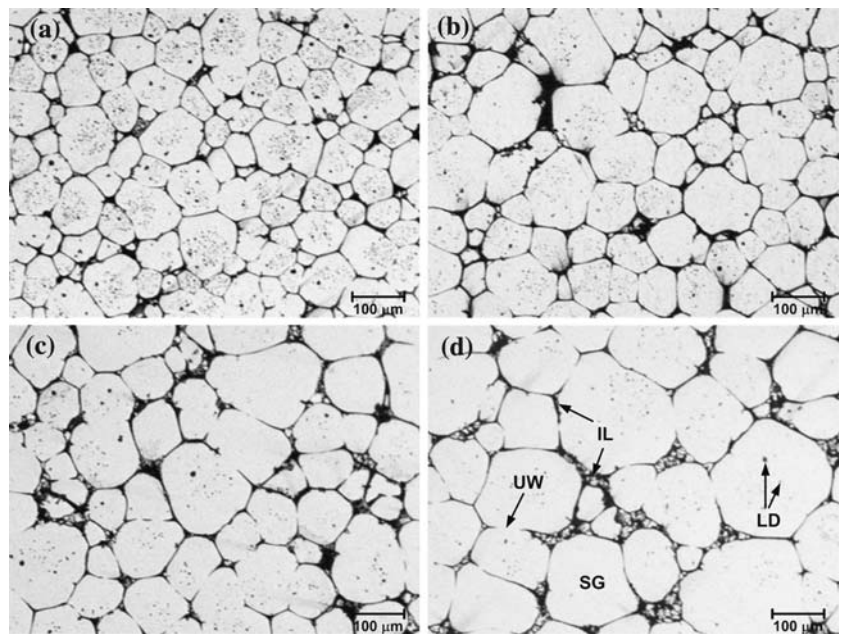
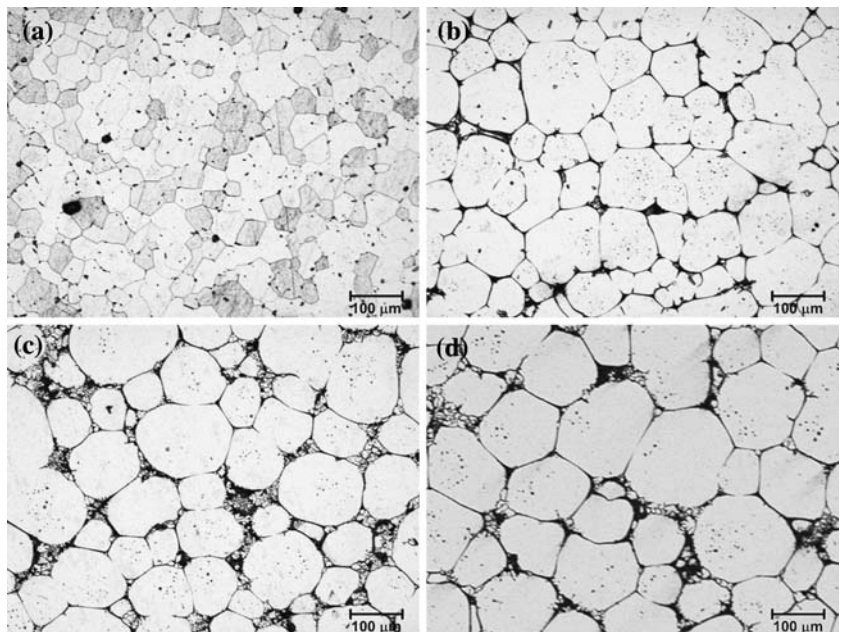


Fig. 3 Optical micrographs of the spray-formed AA7034 alloy quenched after isothermal heat treatment for 120 min at (a) 529 °C ($f_S = 0.90$), (b) 573 °C ($f_S = 0.80$), (c) 595 °C ($f_S = 0.70$), and (d) 607 °C ($f_S = 0.60$)



difficult to measure the exponent n with a high accuracy, most previously determined values of n are approximately 3 for aluminium, copper, and nickel alloys, which is in agreement with the expected value for diffusion-controlled coarsening [7, 8, 13]. In this study, the parabolic and cubic kinetics were both examined for comparison.

Figure 4 shows that the average grain size increases with increasing heat treatment time. At all temperatures the rate of increase of grain size decreases with increasing time. These coarsening data were reconstructed, according to Eq. 1, to plot the grain size to different powers n against heat treatment time. Figure 5 shows plots for (a) $n = 3$ and

(b) $n = 2$, for the data at 529 °C ($f_S = 0.90$), 573 °C ($f_S = 0.80$), 595 °C ($f_S = 0.70$), 607 °C ($f_S = 0.60$), and 615 °C ($f_S = 0.50$). For clarity, only this limited data set is plotted. Regression coefficients, R^2 , for best fits to the data, and the gradients of each best fit line, representing the coarsening rate constant, K , in Eq. 1, are given in Tables 2 ($n = 3$) and 3 ($n = 2$) for the full data set. Except for the value at 529 °C ($f_S = 0.90$), R^2 varies between 0.841 and 0.991 for cubic kinetics, and between 0.831 and 0.986 for parabolic kinetics. Although R^2 values are generally slightly higher for $n = 3$ than $n = 2$, the differences are slight, and it is not possible to ascribe the coarsening

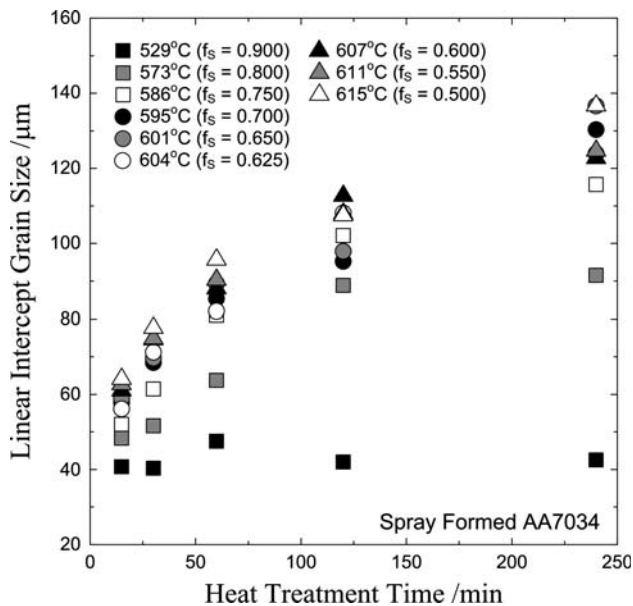


Fig. 4 Plot of mean linear intercept solid grain size of the spray-formed AA7034 quenched after heat treatment at 529–615 °C versus heat treatment time

behaviour with confidence to a particular coarsening exponent. This has been recognised in other studies [11].

The coarsening rate constants, K , determined for each temperature are plotted against solid fraction in Fig. 6 for (a) $n = 3$ and (b) $n = 2$. The overall behaviour of the coarsening rate constant was independent of which exponent, $n = 2$ or 3, was used. Below a solid fraction of 0.6, the coarsening rate constant decreases as the solid fraction increases; for solid fractions between 0.6 and 0.65, the coarsening rate constant increases as the solid fraction increases; and above a solid fraction of 0.65, the coarsening rate constant again decreases as the solid fraction increases.

As mentioned above, previous studies investigating grain coarsening in the semi-solid state generally have reported an exponent of $n = 3$ [7, 8, 13]. Therefore, for the purposes of further analysis, it is assumed in the present study that the grain coarsening was controlled by diffusion in the liquid and followed cubic kinetics ($n = 3$).

Comparison with previous aluminium alloy data

Figure 7 is a plot of the cubic ($n = 3$) coarsening rate constant, K , as a function of solid fraction, f_s , for the spray-formed AA7034 alloy with results from similar studies on grain coarsening in the semi-solid state for other spray-formed aluminium alloys [7, 8, 11]. The chemical compositions of the spray-formed alloys are listed in Table 4 for comparison.

With the exception of the present data for AA7034 and the data for Al-4wt.%Cu collected by Manson-Whitton

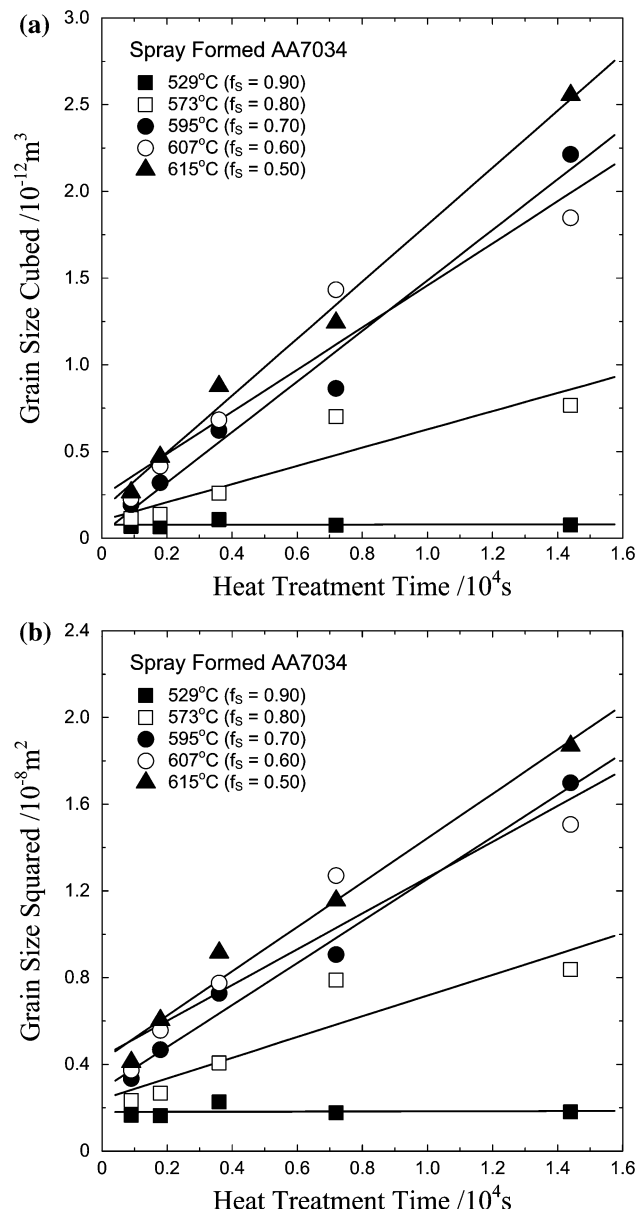


Fig. 5 Plots of mean linear intercept solid grain size (a) cubed and (b) squared as a function of heat treatment time for the spray-formed AA7034 quenched after heat treatment at 529 °C ($f_s = 0.90$), 573 °C ($f_s = 0.80$), 595 °C ($f_s = 0.70$), 607 °C ($f_s = 0.60$), and 615 °C ($f_s = 0.50$)

et al. [11] previous work has been carried out for $f_s \geq 0.65$, i.e., at high solid fractions. For all of the alloys, the coarsening rate constant decreases as the solid fraction increases at such high solid fractions. For the Al-4wt.%Cu alloy of Manson-Whitton et al. [11], data are available over a wider range of solid fraction $0.4 \leq f_s \leq 0.9$, and the coarsening rate constant decreases similarly as the solid fraction increases beyond $f_s = 0.75$. However, the coarsening rate constant increases with increasing solid fraction for $f_s \leq 0.75$.

Table 2 Slopes (K) and regression coefficients (R^2) for linear fits of \bar{d}^n vs. heat treatment time for the spray-formed AA7034 quenched after heat treatment at 529–615 °C with $n = 3$

Temperature (°C)	Solid fraction (f_S)	$K_{n=3}$ ($10^{-18} \text{ m}^3 \text{ s}^{-1}$)	\bar{d}_0^3 (10^{-15} m^3)	R^2
529	0.900	0.182	77.162	0.003
573	0.800	52.540	101.791	0.841
586	0.750	106.195	110.765	0.961
595	0.700	145.754	28.452	0.977
601	0.650	168.928	5.544	0.970
604	0.625	128.931	131.384	0.936
607	0.600	121.392	243.102	0.928
611	0.550	123.992	227.453	0.980
615	0.500	165.615	164.387	0.991

Table 3 Slopes (K) and regression coefficients (R^2) for linear fits of \bar{d}^n vs. heat treatment time for the spray-formed AA7034 quenched after heat treatment at 529–615 °C with $n = 2$

Temperature (°C)	Solid fraction (f_S)	$K_{n=2}$ ($10^{-14} \text{ m}^2 \text{ s}^{-1}$)	\bar{d}_0^2 (10^{-11} m^2)	R^2
529	0.900	0.357	180.151	0.006
573	0.800	47.791	239.545	0.831
586	0.750	78.870	296.823	0.927
595	0.700	96.826	286.445	0.986
601	0.650	107.666	289.860	0.980
604	0.625	88.878	343.608	0.907
607	0.600	82.620	434.716	0.898
611	0.550	83.234	433.015	0.950
615	0.500	102.346	419.864	0.979

Manson-Whitton et al. [11] explained that for solid fractions less than a critical volume fraction ($f_{S0} \approx 0.7$) the coarsening rate is controlled by the thickness of the grain boundary liquid film which decreases with increasing solid fraction (i.e., a decreasing diffusion distance) according to a simple model of liquid film migration:

$$K = \frac{3D_L C_L(\infty)\gamma V_m}{2RT(C_L(\infty) - C_S)(f_S^{-1/3} - 1)} \quad (2)$$

where D_L is the solute diffusion coefficient in the liquid, $C_L(\infty)$, and C_S are the compositions of the bulk liquid and solid, respectively, γ is the solid–liquid interfacial energy, V_m is the molar volume, R is the universal gas constant, T is the absolute temperature, and f_S is the solid fraction.

For solid fractions greater than the critical value, the coarsening rate decreases since the area of grain boundary liquid film decreases. Manson-Whitton et al. [11] developed a modified liquid film migration model to predict the latter behaviour:

$$K = \frac{3D_L C_L(\infty)\gamma V_m(1 - f_S)}{2RT(C_L(\infty) - C_S)(1 - f_{S0})(f_{S0}^{-1/3} - 1)} \quad (3)$$

The AA7034 alloy of the present study behaves in a similar manner to the Al-4wt.%Cu of Manson-Whitton et al. [11] for $f_S \geq 0.6$ with the critical solid fraction, f_{S0} , of 0.65. However, below a solid fraction of 0.6, the coarsening rate constant of spray-formed AA7034 also decreases again as the solid fraction increases from 0.5 to 0.6.

N707 alloy has a similar chemical composition to AA7034, and has approximately the same coarsening rate constants as AA7034 for $0.8 \leq f_S \leq 0.9$. This remarkably good agreement is shown in more detail in Fig. 8. The main solute element of both alloys is zinc, and concentrations of zinc in each alloy are very similar, as shown in Table 4. AA7034 and N707 alloys show lower coarsening rate constants than the other alloys which have copper as their main solute element, with the exception of AA2618 by Grant et al. [7].

Effect of solute diffusion in the liquid

In Fig. 7, the AA7034 and N707 alloys in which zinc is the main solute element, have lower coarsening rate constants than the other aluminium alloys in which copper is the main solute element, except the AA2618 of Grant et al. [7]. These main solute elements can affect the coarsening rate constant due to the difference between their diffusivities in the liquid. Most of the theoretical models [8, 11, 14, 15], including Eqs. 2 and 3, of grain coarsening in the semi-solid state explain that the coarsening rate constant, K , is proportional to the solute diffusion coefficient, D_L , in the liquid:

$$K \propto D_L \quad (4)$$

The diffusivities of zinc and copper in the liquid in the semi-solid temperature region of aluminium alloys have not yet been determined, although they are known in the

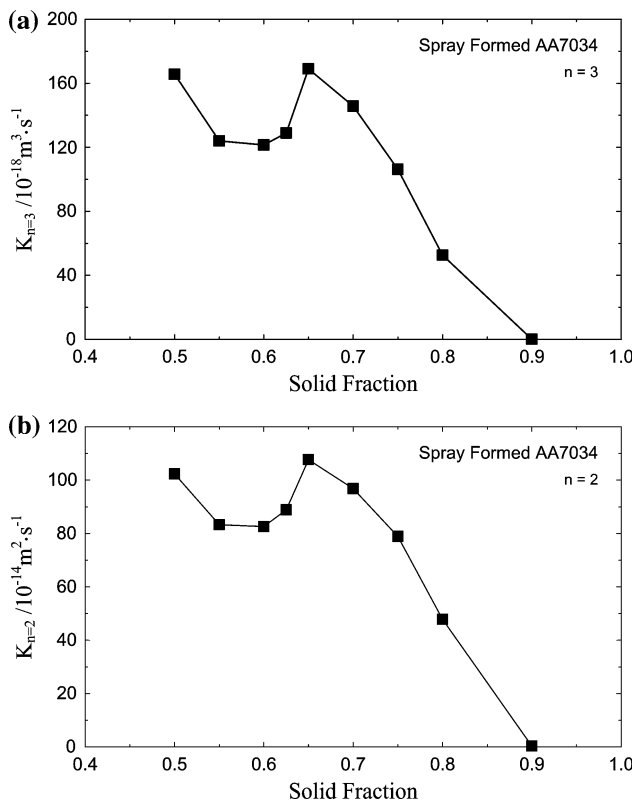


Fig. 6 Plot of coarsening rate constant as a function of solid fraction for the spray-formed AA7034 alloy, assuming (a) cubic kinetics ($n = 3$) and (b) parabolic kinetics ($n = 2$)

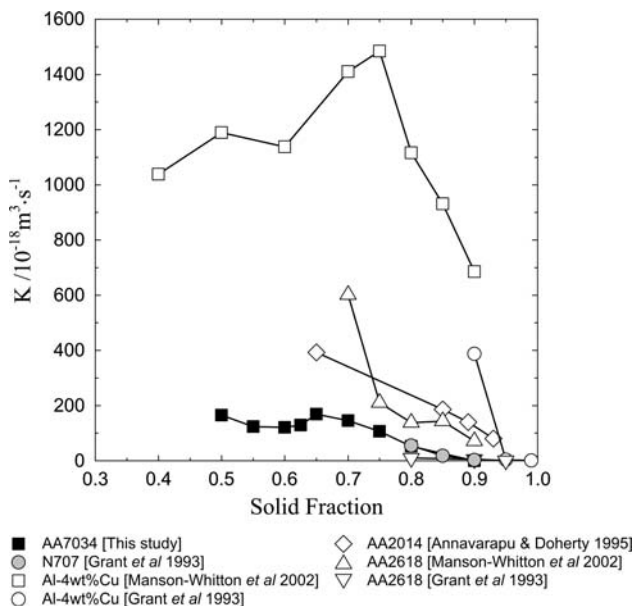


Fig. 7 Plot of cubic coarsening rate constant as a function of solid fraction for the spray-formed AA7034 alloy of this study and for aluminium alloys of other studies [7, 8, 11]

fully liquid state. The diffusivities of copper and zinc in molten aluminium at high temperature are listed in Table 5 [16]. Zinc has a higher diffusivity than copper, but also has

a higher activation energy (68.4 kJ mol^{-1}) than copper (23.8 kJ mol^{-1}) in the high temperature range. Figure 9 is a plot of solute diffusivity as a function of temperature, which is extrapolated from high temperature to the lower semi-solid temperature regime. Although this is not an exact prediction of the diffusivities at low temperature, the diffusivity of copper is expected to exceed that of zinc at temperatures below approximately $676 \text{ }^\circ\text{C}$, i.e., if aluminium could exist as a liquid below its melting point then one would expect copper to diffuse in it more quickly than zinc. Given this hypothesis copper is expected to have a higher diffusivity than zinc in the liquid phase of aluminium alloys in the semi-solid state, and so Al-4wt.%Cu, AA2014, and AA2618 are expected to have higher coarsening rate constants than AA7034 and N707. This account is in agreement with previous theoretical models [8, 11, 14, 15]. The low coarsening rate constants of AA2618 [7] are exceptional and cannot be explained by the solute diffusivity of the main alloying element alone. It is believed that the presence of second-phase dispersoids at the grain boundary liquid films causes this effect, and this will be discussed in the next section.

Effect of second-phase particles at grain boundary liquid films

Annavarapu and Doherty [8] proposed that second-phase particles lying on the grain boundary liquid films inhibit the grain-coarsening process at high solid fraction. Particles which are much smaller than the thickness of the liquid film should provide little barrier to solute transport around them. Their only effect should be to create a small region of negative curvature on the freezing interface. This negative curvature will generate a low-pressure region in the liquid stimulating liquid flow to relieve the pressure and to displace the second-phase particle. On the other hand, particles of sizes comparable to the thickness of the liquid film are likely to inhibit strongly the free migration of the liquid film by becoming a barrier to solute diffusion and fluid flow around them.

Manson-Whitton et al. [11] proposed two possible mechanisms for the sharp increase in coarsening rate constant of AA2618 on the reduction of solid fraction from 0.75 to 0.70, shown in Fig. 7, both concerned with the effect of second-phase particles at grain boundary liquid films. The first is that the second-phase particles dissolve or melt on heating to the slightly higher temperature required for the lower solid fraction, thus unpinning the grain boundary liquid films. The second is that at solid fractions below 0.75 the dispersoids become small relative to the thickness of the liquid films and become ineffective as pinning particles, so that the coarsening rate increases sharply.

Table 4 Concentration of main solute elements for the spray-formed AA7034 alloy of this study and for aluminium alloys of other studies [7, 8, 11]

Alloy	Concentration (wt.%)							
	Zn	Mg	Cu	Cr	Zr	Ni	Fe	Si
AA7034	9.95	2.23	1.20	0.18	0.18	–	0.16	0.04
N707 ^a [7]	10.00	2.00	1.00	–	0.20	–	–	–
Al-4wt.%Cu ^a [7, 11]	–	–	4.00	–	–	–	–	–
AA2014 [8]	0.26	0.71	4.44	0.01	–	–	0.06	0.99
AA2618 ^a [7]	–	1.50	2.60	–	<0.01	1.10	1.10	0.20

^a Nominal compositions

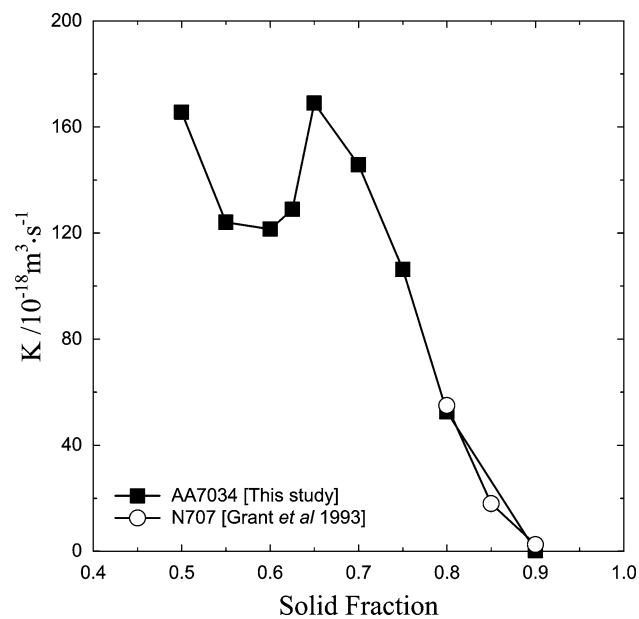


Fig. 8 Plot of cubic coarsening rate constant as a function of solid fraction for the spray-formed AA7034 alloy of this study and for the spray-formed N707 alloys [7]

Table 5 Diffusivities of zinc and copper in molten aluminium [16]

Solute	Temperature		Diffusivity ($10^{-9} \text{ m}^2 \text{ s}^{-1}$)
	K	°C	
Zn	970	697	6.20
	1,073	800	14.00
Cu	1,000	727	6.00
	1,050	777	6.87
	1,100	827	7.78
	1,150	877	8.71
	1,200	927	9.67
	1,250	977	10.63
	1,300	1027	11.61

Figure 10 shows back scattered electron SEM images from second-phase particles in the AA7034 alloy quenched after heat treatment. The particles, labelled A, B, and C,

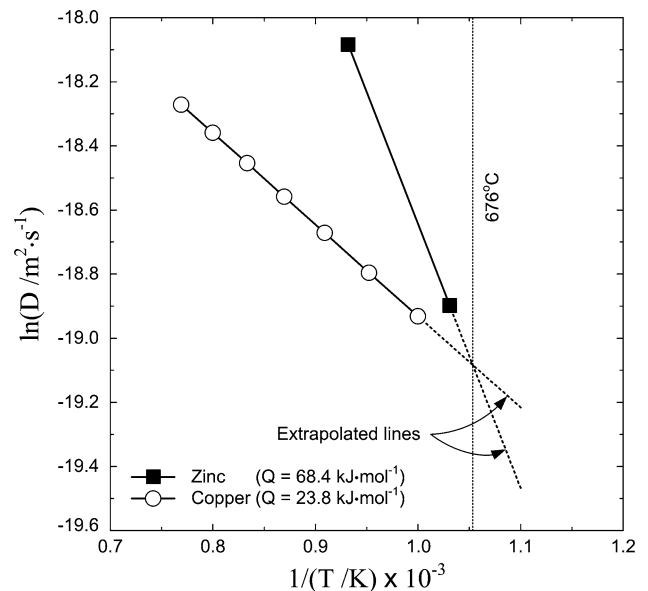


Fig. 9 Plot of diffusivity of zinc and copper in molten aluminium as a function of temperature: $D = D_0 \exp(-Q/RT)$. The dotted lines are extrapolated from the data in Table 6 assuming that the diffusivity variation is linear with temperature

were identified as Al_7Cr , from EPMA analysis of their chemical composition listed in Table 6. Figure 10a shows a particle (A) which was floating in the liquid region, in the alloy quenched after heat treatment for 240 min at 607 °C ($f_s = 0.60$). Although particle A was $\approx 20 \mu\text{m}$ in size, it was relatively small compared with the thickness of the liquid films. This sort of second-phase particle is not expected to be effective in inhibiting the grain coarsening in the semi-solid state, as explained by Annavarapu and Doherty [8] and Manson-Whitton et al. [11].

At high solid fraction, insoluble solid particles have been commonly found at the thin grain boundary liquid films of aluminium alloys, such as AA2014 [8], and AA2618 [11] in the semi-solid state. Additionally, particles (B and C) which are pinning the migrating liquid film between solid grains, in the AA7034 alloy quenched after heat treatment for 120 min at 573 °C ($f_s=0.80$) are shown in Fig. 10b. The thickness of the grain boundary liquid film

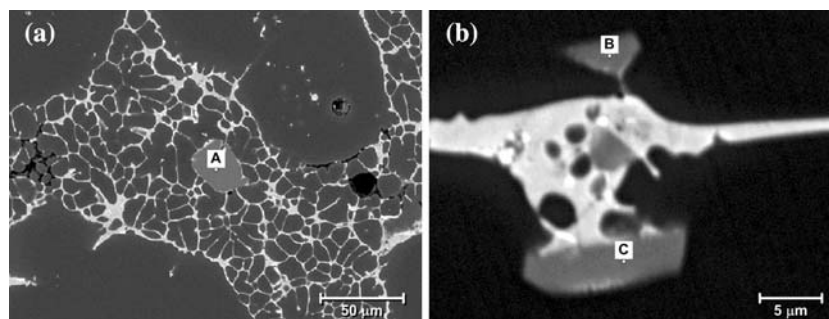


Fig. 10 Back scattered electron SEM images indicating the positions for identification of (a) a particle (labelled A) which was floating in the liquid region, in the AA7034 alloy quenched after heat treatment for 240 min at 607 °C ($f_s = 0.60$), and (b) particles (labelled B and

C) which were pinning the migrating liquid film between solid grains in the AA7034 alloy quenched after heat treatment for 120 min at 573 °C ($f_s = 0.80$)

Table 6 Chemical compositions of the second-phase particles in Fig. 10, analysed using EPMA

Point	Concentration (at.%)							Expected phase
	Al	Zn	Mg	Cu	Cr	Fe	Si	
A	83.27	2.96	0.23	0.34	11.75	1.44	0.04	Al ₇ Cr
B	83.81	2.74	0.20	0.29	11.63	1.08	0.04	Al ₇ Cr
C	84.40	2.63	0.19	0.25	11.47	1.05	0.02	Al ₇ Cr

is much wider where particles are present than at other places, because the second-phase particles might be a barrier to solute transport between the solid grains. Particles B and C cannot easily move with the moving grain boundary liquid films, so inhibiting their migration, and are captured by the growing solid grain. The solid grain appears to be folded around particle B, which confirms that the second-phase particle B is captured. A possible mechanism of inhibition of migration of the grain boundary liquid film by a second-phase particle is depicted in Fig. 11. A second-phase particle at a grain boundary liquid film is captured by migrating interface of a growing solid grain.

AA2014 and AA2618 were expected to have a large amount of insoluble solid particles in the grain boundary liquid films. The effect of the second-phase particles inhibiting the grain coarsening results in significantly lower coarsening rate constants than Al-4wt.%Cu alloy which has either no second-phase particles or just a few impurities. For AA7034 and N707, the coarsening rate seems to be retarded strongly by second-phase particles at very high

solid fractions in addition to the effect of solute diffusivity described in the previous section.

Effect of macroscopic shape change of the specimen

In this study, above a solid fraction of 0.6, the relationship between coarsening rate constant and solid fraction agrees with Manson-Whitton et al.'s model [11]: i.e., for the regime of solid fraction between 0.6 and 0.65, the coarsening rate constant increases as the solid fraction increases; and above the solid fraction of 0.65, the coarsening rate constant decreases as the solid fraction increases. However, below a solid fraction of 0.6, the coarsening rate constant decreases again as the solid fraction increases. This phenomenon cannot be described either by Annavarapu and Doherty's liquid film migration model [8], or by Manson-Whitton et al.'s modified liquid film migration model [11].

Figure 12 shows macroscopic pictures of the AA7034 alloy annealed for 120 min at 601 °C ($f_s = 0.65$), and for 180 min at 615 °C ($f_s = 0.50$). The grain size is fairly

Fig. 11 Possible mechanism of inhibition of migration of a grain boundary liquid film by a second-phase particle. The second-phase particle is captured by the interface of a growing solid grain in the long run

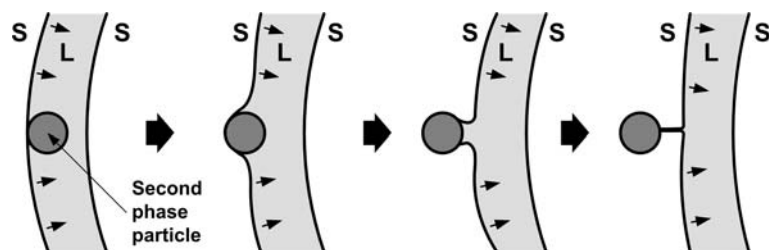
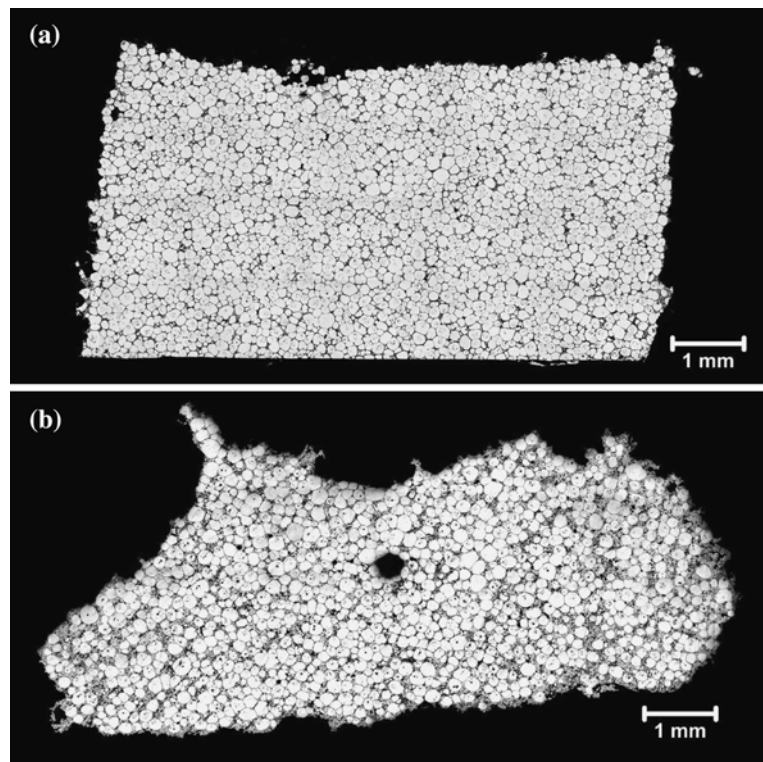


Fig. 12 Macroscopic pictures of the spray-formed AA7034 alloy quenched after the isothermal heat treatment (a) for 120 min at 601 °C ($f_S = 0.65$), and (b) for 180 min at 615 °C ($f_S = 0.50$), showing the shape change during heat treatment. These pictures were made from combinations of tens of pictures



uniform all over the specimen for each sample. At a solid fraction of 0.65, the shape of the specimen remains almost the same during heat treatment as indicated by the approximate rectangular shape in Fig. 12a. At a solid fraction of 0.5, however, the specimen deforms under its own weight during heat treatment, as shown in Fig. 12b. A possible explanation of the coarsening rate constant data at low solid fractions is that the shape change causes liquid flow between the grains, which enhances diffusion, thus accelerating the grain coarsening. Annavarapu and Doherty’s model [8] and Manson-Whitton et al.’s model [11] cannot account for such flow-enhanced diffusion.

In an ideal specimen with a microstructure of perfectly packed equal-sized grains, the grains can be isolated at all solid fractions by a thin liquid film. In practice, the solid grains are often interconnected above some critical solid fraction, and the shape of the specimen remains unchanged under its own weight during heat treatment, as shown schematically in Fig. 13a. However, when the solid fraction is below the critical value, the grains are wholly separated or only partially interconnected, and the specimen deforms under its own weight during heat treatment, as shown in Fig. 13b.

Model formulation of the effect of flow-enhanced diffusion

The proposed flow-enhanced diffusion effect on coarsening occurs when the solid fraction is lower than the critical

value, f_{S0} , and so relates to the regime of coarsening rate constant based on the liquid film migration model in Eq. 2. Combining Eq. 2 with Eq. 4 gives:

$$\bar{r}^3 - \bar{r}_0^3 = \frac{3D_L C_L(\infty)\gamma V_m}{2RT(C_L(\infty) - C_S)(f_S^{-1/3} - 1)} t \tag{5}$$

where \bar{r} is average final grain radius and \bar{r}_0 is the average initial grain radius.

To approximate the effect of flow-enhanced diffusion due to the macroscopic shape change of the specimen during heat treatment, let the coarsening rate constant in Eq. 5 be K_{base} :

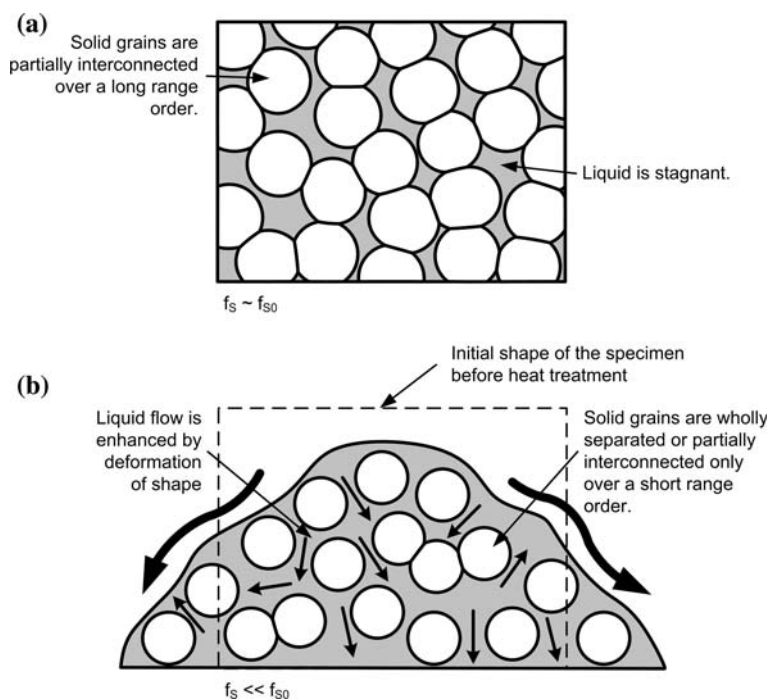
$$K_{base} = \frac{3D_L C_L(\infty)\gamma V_m}{2RT(C_L(\infty) - C_S)(f_S^{-1/3} - 1)} \tag{6}$$

At low solid fraction, the effect of convective mass transfer on diffusion should be included in an effective solute diffusivity in the liquid, D'_L :

$$\begin{aligned} D'_L &= D_L(1 + Pe) = D_L \left(1 + \frac{vF_0}{D_L} \right) \\ &= D_L \left[1 + \frac{vr_0(f_S^{-1/3} - 1)}{D_L} \right] \end{aligned} \tag{7}$$

where Pe is the diffusional Péclet number which is a dimensionless parameter defined by the ratio of convective mass transfer to diffusional mass transfer ($=vF_0/D_L$), v is the velocity of the liquid, $F_0 = r_0 (f_S^{-1/3} - 1)$ is the

Fig. 13 Schematic pictures showing (a) that a specimen keeps its shape during heat treatment since the solid grains are partially interconnected in a long-range order when f_S is slightly lower than the maximum packing ratio, f_{S0} , (b) that the specimen deforms under its own weight during the heat treatment since the solid grains are wholly separated or partially interconnected only in a short-range order when f_S is significantly lower than f_{S0}



thickness of the grain boundary liquid film, and r_0 is the initial radius of the solid grains. Note that the diffusional Péclet number is not independent of solid fraction, f_S , and heat treatment time.

If it is assumed that the height of the specimen, h , decreases exponentially with time, t , then:

$$h = h_0 \exp\left(-\frac{t}{\tau}\right) \quad (8)$$

where h_0 is the initial height of the specimen, and τ is the characteristic time for exponential decay, which is a function of apparent viscosity in the semi-solid state η_a , and the stress due to the weight of the specimen σ_{self} :

$$\tau = \frac{\eta_a}{\sigma_{\text{self}}} \quad (9)$$

In the semi-solid state, the viscosity is assumed to vary with solid fraction, f_S , as follows [17]:

$$\eta_a = A_1 \exp A_2 f_S \quad (10)$$

where A_1 and A_2 are structural parameters.

The velocity of the top surface, v_s , of the specimen is defined as the differential of the height, h , with respect to time, t :

$$v_s = -\frac{dh}{dt} = \frac{h_0}{\tau} \exp\left(-\frac{t}{\tau}\right) = \frac{h}{\tau} \quad (11)$$

Then the relative velocity, v , of the liquid flowing between the two solid grains, which can give an effect on the solute transport in the liquid, is defined as a linear function of v_s .

$$v = A_3 v_s = A_3 \frac{h_0}{\tau} \exp\left(-\frac{t}{\tau}\right) \quad (12)$$

Replacing the solute diffusivity, D_L , in the liquid with the effective solute diffusivity, $D'_L (= D_L(1 + Pe))$, in the liquid in Eq. 6, the coarsening rate constant is altered to an effective coarsening rate constant, K' , instead of K_{base} to account for the effect of convection:

$$K' = \frac{3D'_L C_L(\infty) \gamma V_m}{2RT(C_L(\infty) - C_S)(f_S^{-1/3} - 1)} \quad (13)$$

or, substituting D'_L with Eq. 7:

$$K' = \frac{3D_L C_L(\infty) \gamma V_m}{2RT(C_L(\infty) - C_S)(f_S^{-1/3} - 1)} \left[1 + \frac{vr_0(f_S^{-1/3} - 1)}{D_L} \right] \\ = K_{\text{base}} \left[1 + \frac{vr_0(f_S^{-1/3} - 1)}{D_L} \right] \quad (14)$$

where $v = A_3 (h_0/\tau) \exp(-t/\tau)$, $\tau = \eta_a/\sigma_{\text{self}}$, and $\eta_a = A_1 \exp A_2 f_S$. Note that the effective coarsening rate constant, K' , in Eq. 13 is a function of time. As time increases, the relative velocity, v , approaches zero, and K' approaches K_{base} .

The coarsening rate constant predicted qualitatively using Eq. 13 is plotted in Fig. 14 as a function of solid fraction, f_S , for the flow-enhanced diffusion model in conjunction with the previous liquid film migration and modified liquid film migration models by Manson-Whitton et al. [11], for $f_{S0} = 0.7$. It is not possible to use this model

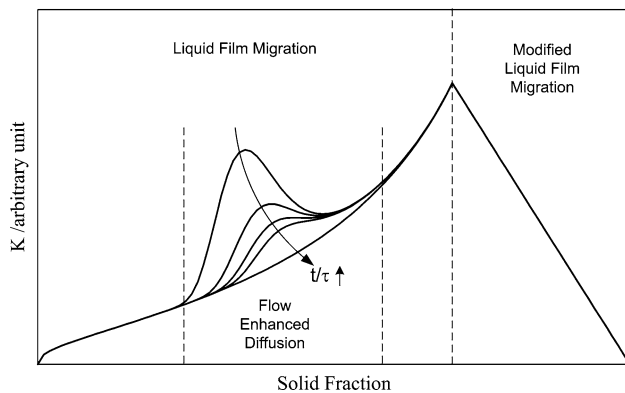


Fig. 14 Predicted coarsening rate constant as a function of solid fraction for flow-enhanced diffusion model with liquid film migration and modified liquid film migration model, for $f_{S0} = 0.7$. As time increases, the curve approaches to the liquid film migration model

in a quantitative manner because a number of the physical properties such as viscosity and solid–liquid interfacial energy in the semi-solid state are not known. Thus it is difficult to compare the theoretical and experimental results in this study. The coarsening rate constant decreases with increasing solid fraction for $f_{S0} < f_S < 1.0$, and increases with increasing solid fraction for $0 < f_S < f_{S0}$, as explained by Manson-Whitton et al. [11], except in the region of flow-enhanced diffusion. In that region, the effective solute diffusivity becomes higher due to flow-enhanced diffusion, and thus the coarsening rate constant is higher than that estimated by the liquid film migration model.

The exaggeration of coarsening rate constant is more significant as heat treatment time, t , decreases, as shown in Fig. 14. This means that flow-enhanced diffusion is more active in the initial stages of heat treatment. As the heat treatment time increases, the effect of flow-enhanced diffusion decreases, and the curve approaches the normal liquid film migration model.

Summary of models for grain coarsening in the semi-solid state

The explanation of flow-enhanced diffusion, liquid film migration, and modified liquid film migration, is summarised in Fig. 15:

- *Liquid film migration model* ($0.0 < f_S < f_{S0}$) [11]
In the regime L, the coarsening rate increases with increasing solid fraction, according to Eq. 2, since the thickness of the grain boundary liquid film decreases and thus the diffusional distance between the grains decreases.
- *Modified liquid film migration model* ($f_{S0} < f_S < 1.0$) [11]

In the region M, the coarsening rate decreases with increasing solid fraction, according to Eq. 3, since the area of liquid film reduces with increasing solid fraction.

- *Flow-enhanced diffusion model*

In the region F, which is included in the region L, the coarsening rate constant increases and then decreases with increasing solid fraction, according to Eq. 14 and the coarsening rate constant is higher than that estimated by the liquid film migration model, since the macroscopic shape change of specimen induces convective mass transfer of solutes in the grain boundary liquid film.

Conclusions

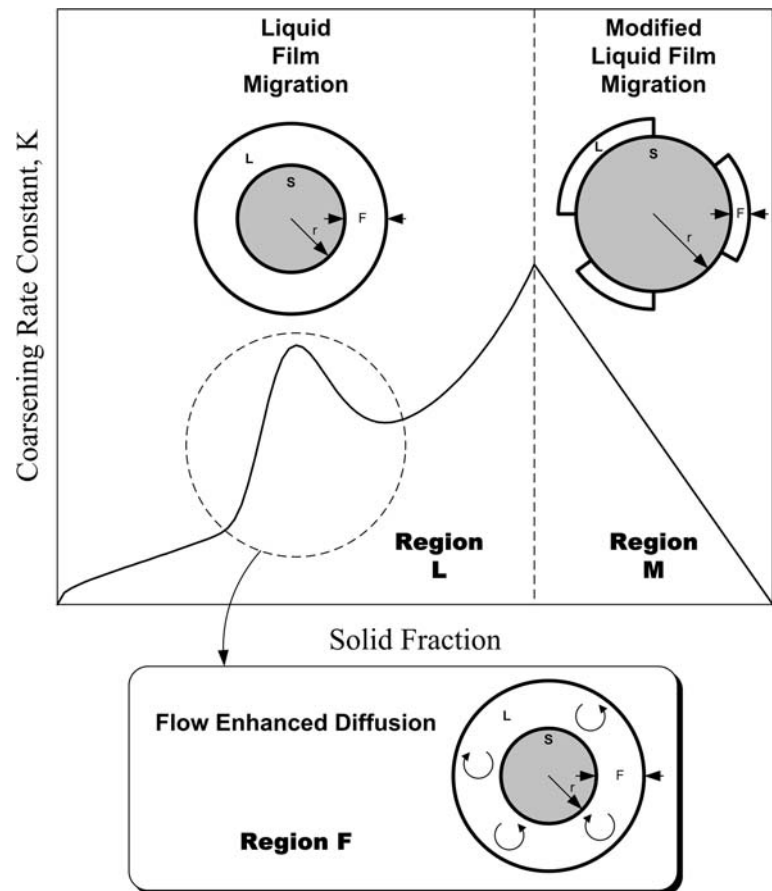
The kinetics of semi-solid grain coarsening in a spray-formed AA7034 aluminium alloy over a wide range of solid fractions has been studied by the use of ex situ coarsening experiments.

Generally, aluminium alloys with zinc as a main solute element, such as AA7034 and N707, have lower coarsening rate constants than aluminium alloys with copper as a main solute element. This is because the diffusivity of copper is expected to be higher than that of zinc in the liquid phase in the semi-solid state temperature range, and the coarsening rate constant is known to be proportional to the solute diffusivity. At high solid fraction, insoluble second-phase particles are present at the thin grain boundary liquid films in AA7034 in the semi-solid state, inhibiting grain coarsening in the semi-solid state.

The coarsening rate constant of the spray-formed AA7034 alloy decreases with increasing solid fraction for $f_S > 0.65$. For $0.6 < f_S < 0.65$, the coarsening rate constant increases as the solid fraction increases. For $f_S < 0.6$, the coarsening rate constant decreases again with increasing solid fraction. The phenomenon for solid fractions below 0.6 is not in agreement with previous studies. A macroscopic shape change takes place during annealing, causing liquid flow between the grains, which enhances diffusion and grain coarsening. When the solid grains are interconnected, the shape of the material remains unchanged under its own weight during heat treatment. However, when the solid fraction is very low, the grains are wholly separated, or only partially interconnected, and the material can deform under its own weight during heat treatment.

A model of flow-enhanced diffusion has been developed to explain the grain-coarsening behaviour of the spray-formed AA7034 at low solid fractions, considering the liquid velocity and characteristics of the macroscopic shape change. Together with the liquid film and modified liquid film migration models, the flow-enhanced diffusion model

Fig. 15 Schematic plot of coarsening rate constant as a function of solid fraction, showing the regions of liquid film migration (L), modified liquid film migration (M), and flow-enhanced diffusion (F), with schematic diagram of a solid grain of radius, r , surrounded by a liquid film of thickness, F . In region M, film thickness remains constant but solid area in contact with liquid reduces. In region L, film thickness decreases as the solid fraction increases. In region F, solute diffusion is enhanced by liquid flow due to macroscopic shape change of the specimen



shows qualitative agreement with available experimental results. The effect of the flow-enhanced diffusion disappears when there is no macroscopic shape change.

References

1. Flemings MC (1991) Metall Trans A 22:957
2. Kirkwood DH (1994) Int Mater Rev 39:173
3. Han DS (2000) DPhil Thesis. University of Oxford
4. Grant PS (1995) Prog Mater Sci 39:497
5. Mathur P, Apelian D, Lawley A (1989) Acta Metall 37:429
6. Mathur P, Annavarapu S, Apelian D, Lawley A (1991) Mater Sci Eng A 142:261
7. Grant PS, Underhill RP, Kim WT, Mingard KP, Cantor B (1993) ICSF 2:45
8. Annavarapu S, Doherty RD (1995) Acta Metall Mater 43: 3207
9. Pedneau N, Peguleryuz MO (1997) Scripta Mater 37:903
10. Wolfsdorf TL, Bender WH, Voorhees PW (1997) Acta Mater 45:2279
11. Manson-Whitton ED, Stone IC, Jones JR, Grant PS, Cantor B (2002) Acta Mater 50:2517
12. Kim HS (2003) DPhil Thesis. University of Oxford
13. Underhill RP, Grant PS, Bryant DJ, Cantor B (1995) J Mater Synth Process 3:171
14. Lifshitz IM, Slyozov VV (1961) J Phys Chem Solids 19:35
15. Wagner C (1961) Z Elektrochem 65:581
16. CRC handbook of chemistry and physics (2004) Website, CRC Press. <http://www.hbcpnetbase.com>, Accessed 15 November 2007
17. Joly PA, Mehrabian R (1976) J Mater Sci 11:1393